Numerical Heat Transfer, Part A, 51: 267–291, 2007
Copyright © Taylor & Francis Group, LLC
ISSN: 1040-7782 print/1521-0634 online
DOI: 10.1080/10407780600710250

Taylor & Francis
Taylor & Francis Group

NUMERICAL SIMULATION OF FLOW AND HEAT TRANSFER IN ROUND-TO-RECTANGULAR NOZZLES

Jun-Wei Li, Yu Liu, and Li-Zi Qin
School of Astronautics, Beijing University of Aeronautics and Astronautics, Beijing, People's Republic of China

Fluid flow and heat transfer in three-dimensional round-to-rectangular (RR) nozzles with regenerative cooling are analyzed numerically. In this analysis, the hot gas flow in the nozzle and the coolant flow in the cooling channels are taken into account, and the heat transfer processes of convection, radiation, and conduction are included. The characteristics of the RR nozzle are obtained. Effects of structure parameters on the flow and heat transfer of the RR nozzle are investigated. The parameters are round-to-rectangular transforming position, height-to-width ratio at the outlet, and arc radius of the outlet. The results indicate that the RR nozzle has different flow features than an axisymmetric nozzle; the height-to-width ratio of the exit plane has a significant influence on the flow and heat transfer in RR nozzles.

1. INTRODUCTION

The increasing demand for the transportation of payloads into earth orbit and the increasing weight of payloads poses a challenge for the development of new launch systems and more powerful liquid rocket engines (LREs). To make rocket engines more powerful, the chamber temperature and pressure in LREs must be higher, which exceeds by far the safe operation temperature of all conventional liner materials currently in use. In order to assure adequate life of the combustion chamber walls (liner), active cooling is required. Typical high-performance rocket engines such as the Space Shuttle Main Engine (SSME) [1], the European HM7, and Vulcain engines [2] use regenerative cooling. To cool the walls of such rocket engines, a cryogenic fuel or oxidizer is passed through cooling channels that are machined evenly around the liner and enclosed on the outside by an electrochemically deposited nickel layer. The liner is usually made of high-conductivity copper alloy. In order to make the rocket engine reliable and reusable, the wall temperature should be maintained below the material's thermal limit. Therefore, the prediction of heat transfer characteristics in a high-performance combustion chamber is one of the most important and challenging tasks in designing a rocket engine.

Before the wide availability of high-speed computers, one-dimensional Nusselt-Reynolds heat transfer correlations, on both the hot gas side and the coolant side,

Received 11 February 2005; accepted 22 February 2006.
Address correspondence to Jun-wei Li, School of Astronautics, Beijing University of Aeronautics and Astronautics, Beijing 100083, People's Republic of China. E-mail: david78lee@sina.com

NOMENCLATURE

$\boldsymbol{A}$	surface area vector, m^2	κ	absorption coefficient, 1/m
C	constant	μ	viscosity, kg/m s
C_p	specific heat at constant pressure, J/kg K	$\boldsymbol{v}$	Velocity vector (u, v, w), m/s
G	production term, $kg/m\,s^3$	ρ	density, kg/m^3
I	radiative intensity	σ	scattering coefficient, 1/m
I_{sp}	specific impulse, m/s	σ_k, σ_ε	turbulent Prandtl number
k	turbulence kinetic energy, m^2/s^2	ϕ	transported variable (ρ, u, v, w, e)
P	chamber pressure, MPa	$\nabla\phi$	gradient of ϕ
S	source term	Φ	scattering phase function
T	temperature, K	$\boldsymbol{\Omega}$	direction vector
α	absorption coefficient, 1/m		
γ	specific heat ratio of gas	**Subscripts**	
Γ_ϕ	diffusion coefficient for ϕ	b	buoyancy
ε	emissivity	g	gas
ε	dissipation rate, m^2/s^3	t	turbulent
η	efficiency	w	wall

were used for computing the heat transfer rates between the hot gas and the wall of the nozzle. Bartz's equation [3] is such a correlation and was widely used for the calculation of the heat transfer coefficients. Marchi et al. [4] proposed a one-dimensional mathematical model, taking into account the effects of area and properties, the shearing stress produced by viscous forces, and the heat transfer to the wall by convection and radiation.

In recent years, computational fluids dynamics (CFD) tools have been developed to allow two-dimensional and even three-dimensional flow and associated heat transfer calculations. These tools are used both for hot-gas-side and coolant-side flow calculations. Since they are numerically complex, these codes cannot yet be used for daily engineering design work, but are rather employed for the analysis of special flow and heat transfer effects [5]. Using CFD tools, Wang et al. [6, 7] investigated the heat transfer on the hot-gas wall and the coolant wall in an axisymmetric nozzle, and also conducted computational analysis to study the linear aerospike plume-induced base-heating physics and fence effect. Fröhlich et al. [8] and Le Bail and Popp [9] studied numerically the flow and heat transfer in channels with high aspect ratio. Knab et al. [10] applied CFD software to the design of the Ariane5 main engine VINCI. Employing large-eddy simulation and a turbulence model, Park [11] investigated the geometric effects on the local heat transfer in a calorimetric chamber.

However, most of the above studies focused on the flow and heat transfer of axisymmetric nozzles. None of these studies dealt with the flow and heat transfer in round-to-rectangular nozzles (RR nozzles). Since the RR nozzle is axisymmetric before the throat and then becomes rectangular, it is very suitable for linear plug nozzles [12, 13]. The special structure of the RR nozzle makes its flow and heat transfer unique. The flow structure of the hot gas in the RR nozzle is three-dimensional, which leads to a three-dimensional distribution of the temperature and heat flux on the gas-side wall.

In this study, three-dimensional numerical simulations of RR nozzles are carried out using the commercial CFD software Fluent 6.0 with a user-defined function. Three-dimensional Navier-Stokes equations are solved to compute the flow and heat transfer in the RR nozzles, taking into account the heat transfer from the hot gas to the wall and from the channels to the coolant. The heat transfer characteristics in the RR nozzle are obtained. In addition, the effects of the geometries on the performance and the heat transfer of these RR nozzles are investigated, including round-to-rectangular transforming location, height-to-weight ratio, and corner radius.

2. PHYSICAL MODEL

The structure of an RR nozzle is shown in Figure 1*a*. It is axisymmetric upstream to a certain position and then becomes rectangular after this point. The cross section after transforming is a closed rectangle, whose four corners are replaced by four quarter-circles in which the circle radii vary with the centerline. In the process of designing, three generatrix functions are adopted to describe the three-dimensional contour of an RR nozzle. By controlling these functions, smooth conversion from round to rectangular cross section can be ensured. These three functions are variations of the intersection of the gas-side wall and the XY plane, the intersection of the gas-side wall and the XZ plane, and the intersection of the corner radius with the centerline.

An RR nozzle is selected as a baseline, and its structural parameters are specified as follows. The throat diameter is 49 mm, and the convergent and divergent ratios are both 5.5. The lengths of the convergent and divergent segments are 104.55 mm and 159.8 mm, respectively. The exit plane has a height-to-width ratio of 0.8 and a corner radius of 22 mm. The baseline transforms at 10% divergent length downstream of the throat. The baseline has a proper height-to-weight ratio and corner radius, and does not make the plug nozzles in which the baseline is installed too wide in geometry. Several structural parameters are varied and their influences on flow and heat transfer in RR nozzles are studied.

Regenerative cooling structure in an RR nozzle consists of liner, ribs, cooling channels, and outer jacket, as shown in Figure 1*a*. In the calculations, it is assumed that the heat transferred from the gas to the gas-side wall is all absorbed by coolant, and the outer wall of the jacket is an adiabatic wall. There are 68 cooling channels around each nozzle, and the width of all ribs between cooling channels is equal to 1.3 mm, remaining the same along the centerline. All RR nozzles in the following section have the same channel number and wall thickness as the baseline nozzle. Liner thickness is 0.8 mm, and outer jacket thickness is 2 mm. Cooling channels have a height of 2 mm, and the width varies with centerline.

3. NUMERICAL PROCEDURE

To simplify the physical model, this work investigates flow and cooling only in the RR nozzle, not taking into account the process in the combustion chamber. The RR nozzle uses liquid oxygen and liquid hydrogen as propellants, liquid hydrogen as coolant. The high-temperature gas in the RR nozzle is a mixture of the combustion products of LOX/LH2. The thermophysical properties of the mixture are the

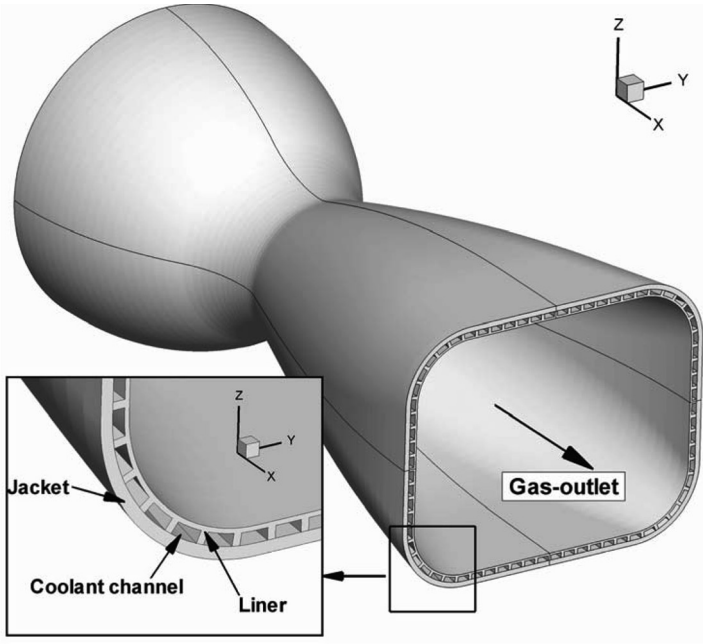

(*a*)

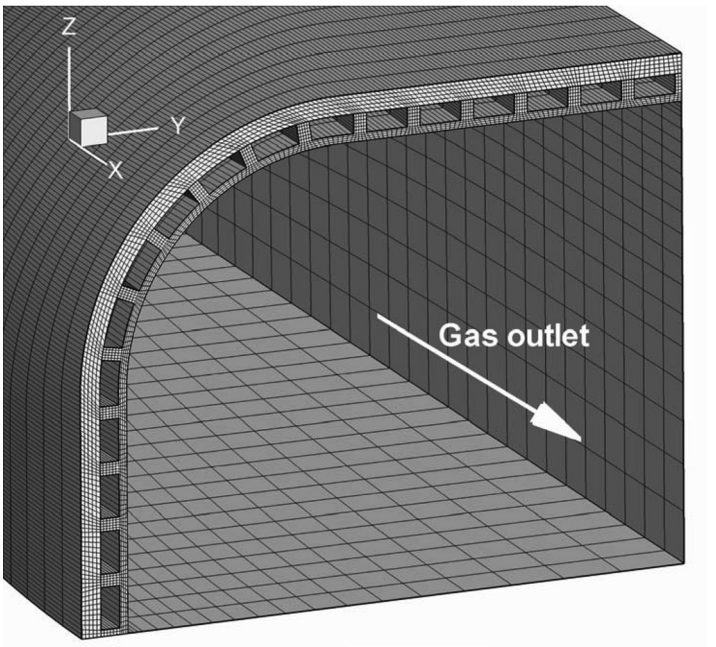

(*b*)

Figure 1. (*a*) RR nozzle model with cooling channels; (*b*) Computational grid of the nozzle.

weighted average of every species, which come from thermodynamic calculation. Because of fast decline of temperature and pressure at the nozzle divergence section, the fluid flow in the RR nozzle is assumed frozen and therefore species in combustion products do not change chemically. Since the heat transfer process in the RR nozzle includes convection, radiation, and conduction, the discrete ordinates (DO) radiative model, Navier-Stokes equations, and the standard $k - \varepsilon$ turbulent model are employed.

3.1. Couple Model of Flow and Heat Transfer

The temperature values on the wall and heat flux through the wall in the RR nozzle are unknown when running the engine. In order to obtain the gas-wall temperature, it is necessary to simultaneously solve the forced convection from the gas to the internal wall, wall conduction, and the convection from the channel wall to the coolant. The adopted governing equations are integral equations over an arbitrary control volume, as follows:

$$\oint \rho\phi \boldsymbol{v} \cdot d\boldsymbol{A} = \oint \Gamma_\phi \nabla\phi \cdot d\boldsymbol{A} + \int_V S_\phi \, dV \tag{1}$$

where ϕ is the transported variable; ρ is the density; $\boldsymbol{v}$ represents the velocity vector; $\boldsymbol{A}$ denotes the surface area vector; Γ_ϕ represents the diffusion coefficient for ϕ; $\nabla\phi$ is the gradient of ϕ; and S_ϕ is the source of ϕ per unit volume.

The above equation can be used to solve convective and conductive problems. When ϕ includes (ρ, u, v, w, e), the above equation can be used to compute the hot gas flow and the coolant flow, comprising the mass conservation equation, the momentum equations, and the energy equation. When ϕ is internal energy, the above equation is an energy equation and can be used to compute heat conduction inside the nozzle wall. The coupling of flow and heat transfer occurs on the gas wall and the liquid wall, satisfying requirements of the coupled surface which include temperature continuity and heat flux continuity.

3.2. Radiative Transfer Model

The radiative transfer equation (RTE) in a Cartesian coordinate system can be expressed as the balance of energy passing in a specified direction Ω through a small differential volume in an absorbing, emitting, and scattering gray medium, as [14]

$$(\boldsymbol{\Omega} \cdot \boldsymbol{\nabla}) I(\boldsymbol{r}, \Omega) = -(\kappa + \sigma) I(\boldsymbol{r}, \Omega) + \kappa I_b(\mathbf{r}) + \frac{\sigma}{4\pi} \int_{\Omega'=4\pi} I(\boldsymbol{r}, \Omega') \Phi(\Omega' \to \Omega) d\Omega' \tag{2}$$

The discrete ordinates method is adopted, which solves the RTE numerically along discrete directions that approximate angular intensity distribution. This method shares the same philosophy and computational grid as the control-volume CFD approach.

The radiation characteristics of water vapor are different from those of the solid and liquid. Water vapor is selective for wavelength, and radiates only in some

wavelength range. Accordingly, it can absorb in the same wavelength range. Hence it cannot be considered as a gray surface. In order to consider the selectivity of water vapor, an averaged emissivity method is used in this study. Consequently, all of the variables in the RTE are changed to total parameters in full spectrum and there are no monochromatic variables, which makes the RTE easy to solve.

Solving the RTE is required to know the absorption coefficient of water vapor. In the past, the coefficient was obtained from Hottel's zonal method, but this method is inconvenient for engineering application and numerical computation. Therefore, Leckner's formula [15], obtained from the narrow-band model, is used in this study as follows:

$$\frac{\varepsilon}{\varepsilon^*} = \exp\left[-\xi(\eta_{\max} - \eta)^2\right]\left(\frac{Ap_e + B}{p_e + A + B - 1} - 1\right) + 1 \tag{3}$$

where $\eta = \log_{10}(p_i L)$; ε^* is emissivity when the equivalent pressure equals 1, obtained from

$$\ln \varepsilon^* = a_0 + \sum_{i=1}^{2} a_i \eta^i \qquad a_i = c_{0i} + \sum_{j=1}^{2} c_{ji}\tau^j \tag{4}$$

where $\xi, \eta_{\max}, A, B,$ and p_e are variables in the above equation, a_i and c_{ji} are coefficients from the formula fitted with original data. They are only symbols and have no real physical meaning.

Additionally, the following equation can approximate the relationship between absorption coefficient and emissivity of the combustion gas [16]:

$$\frac{\alpha_g}{\varepsilon} = \left(\frac{T_g}{T_w}\right)^{1.5} \tag{5}$$

where T_g is gas temperature and T_w is gas wall temperature.

3.3. Turbulence Model

Because of high Reynolds number in the RR nozzle flow field, the flow and the heat transfer cannot be assumed to be laminar but must be considered to be turbulent. The standard $k-\varepsilon$ model is used in this study. Turbulent kinetics energy k and dissipation rate ε can be obtained from the following transport equations [17]:

$$\frac{\partial}{\partial t}(\rho k) + \frac{\partial}{\partial x_i}(\rho k u_i) = \frac{\partial}{\partial x_j}\left[\left(\mu + \frac{\mu_t}{\sigma_k}\right)\frac{\partial k}{\partial x_j}\right] + G_k + G_b - \rho\varepsilon - Y_M + S_k \tag{6}$$

$$\frac{\partial}{\partial t}(\rho\varepsilon) + \frac{\partial}{\partial x_i}(\rho\varepsilon u_i) = \frac{\partial}{\partial x_j}\left[\left(\mu + \frac{\mu_t}{\sigma_\varepsilon}\right)\frac{\partial \varepsilon}{\partial x_j}\right] + C_{1\varepsilon}\frac{\varepsilon}{k}(G_k + C_{3\varepsilon}G_b) - C_{2\varepsilon}\rho\frac{\varepsilon^2}{k} + S_\varepsilon \tag{7}$$

In these equations, G_k represents the production of turbulence kinetic energy due to the mean velocity gradients. G_b is the production of turbulence kinetic energy

due to buoyancy. Y_M represents the contribution of the fluctuating dilatation in compressible turbulence to the overall dissipation rate. $C_{1\varepsilon}, C_{2\varepsilon}$, and $C_{3\varepsilon}$ are constants. σ_k and σ_ε are the turbulent Prandtl numbers for k and ε, respectively. S_k and S_ε are source terms.

Turbulent viscosity μ_t is computed from k and ε as follows:

$$\mu_t = \rho C_\mu \frac{k^2}{\varepsilon} \tag{8}$$

where C_μ is a constant. The values of constants in the standard $k-\varepsilon$ two-equation model are $C_{1\varepsilon} = 1.44$, $C_{2\varepsilon} = 1.92$, $C_\mu = 0.09$, $\sigma_k = 1.0$, and $\sigma_\varepsilon = 1.3$.

3.4. Numerical Method

The working conditions in the RR nozzle with regenerative cooling are complex. They include supersonic flow of the hot gas as well as incompressible flow of the coolant. This makes it difficult to achieve convergence when solving Eq. (1) using a coupled method. As a consequence, time-derivative preconditioning is performed for these equations and the derivative of pressure with respect to time is added to these equations, which introduces the coupling of pressure and velocity. This method enhances stability and increases convergence speed when solving low-Mach-number flow, while not affecting convergent efficiency when solving supersonic flow.

In this study, a time-marching scheme and the control-volume method are employed to solve nonchemical transport equations. The convective terms in coupled equations are discretized with the second-order upwind scheme and viscous terms are discretized with the second-order central difference scheme.

When solving these equations, the temperature on the gas-side wall is initially assigned a value and then gas absorption coefficients are computed until they converge. The obtained temperature on the gas-side wall is regarded as a known value with which to calculate the gas absorption coefficients and to solve the governing equations. Iteration is carried out several times and then ended if the temperature in two consecutive iterations does not change.

3.5. Boundary Conditions

The following boundary conditions are required in the calculation.

1. The inlet boundary is applied to the hot-gas and coolant entrances. At the hot-gas inlet boundary, total temperature and total pressure are fixed. At the coolant inlet boundary, coolant mass flow rate and static temperature are fixed. The turbulent intensity and characteristic length are given as turbulence condition. The radiation condition is internal emissivity.
2. The outlet boundary is used at the hot-gas outflow and coolant outlet. At these two boundaries, back flow pressure and temperature are given. The turbulent condition and radiation condition are the same as for the inlet boundary.

3. The wall boundary is divided into two groups, coupled wall and uncoupled wall. Coupled wall refers to gas/solid or liquid/solid wall and is a non-slip wall. The gas side wall is a coupled wall, whose material is copper alloy and whose emissivity is 0.7. The uncoupled wall is an adiabatic wall.
4. The symmetric boundary includes two sides of the hot gas region, the symmetric plane of the coolant channel, and two sides of the gas walls.

3.6. Computational Grids

In order to compare the computational results, all RR nozzles in this work have the same grid and grid distribution. To reduce the computational time, the RR nozzle is divided into several regions and each region is meshed individually. Because the gas region is wedge-shaped, it is meshed with wedge volume elements; the cooling structure is meshed with hexagonal volume elements. Finally, two zones are coupled by using temperature and heat flux. The grid number of the gas flow region is 108,000, and of the cooling structure is 230,000. To simulate boundary flow and heat transfer, a finer grid is adopted near the gas-side wall and the coolant-side wall. In addition, a standard wall function is used to decrease grid number at the boundary. The computational grids are shown in Figure 1*b*.

4. NUMERICAL VALIDATION

Numerical simulation was carried out for the test combustor in [18–21]. The throat diameter of the combustor is 50.6 mm, the combustor wall material is CuAgZr alloy, and the thickness of the gas wall is 0.7 mm. The coolant is water, and chamber pressure is 10.2 MPa. Propellants are LOX and LH2, mixture ratio $O/F = 6$. With these parameters, thermodynamics software was used to obtain combustor temperature, specific heat ratio, and mean molecular weight of the combustion gas. The thermophysical data for water are fitted as a function of temperature. Because of no conductivity function of CuAgZr alloy with temperature, its conductivity was assumed constant [22]. To save computational time, the combustor was divided into many parts according to the number of cooling channels, and then half of the partitioned part was simulated. The computational model of the test combustor is shown in Figure 2*a*.

Heat flux distribution on the gas-side wall along the axis is shown in Figure 2*b*. Horizontal coordinates represent the axis of the nozzle, and the origin is located at the throat. The vertical axis represents heat flux through the gas-side wall. The results from CryoROC software [18] and results computed in this article were compared in Figure 2*b*. The CryoROC software can solve the entire flow field within a rocket chamber, taking into account complex physical phenomena. CryoROC results agreed well with test results under other conditions in [18]. Consequently, it is proper to verify the method in this study using CryoROC results as a benchmark.

At the inlet and the outlet of the nozzle, heat flux computed in this study is higher than that of CryoROC in Figure 2*b*. At the throat, the two results are very close. The reason is that gas-wall thickness of the test engine varies along the axis, while the model in this study has a uniform thickness along the axis. In Figure 2*b*, it is shown that radiative heat flux on the gas wall decreases along the axis and

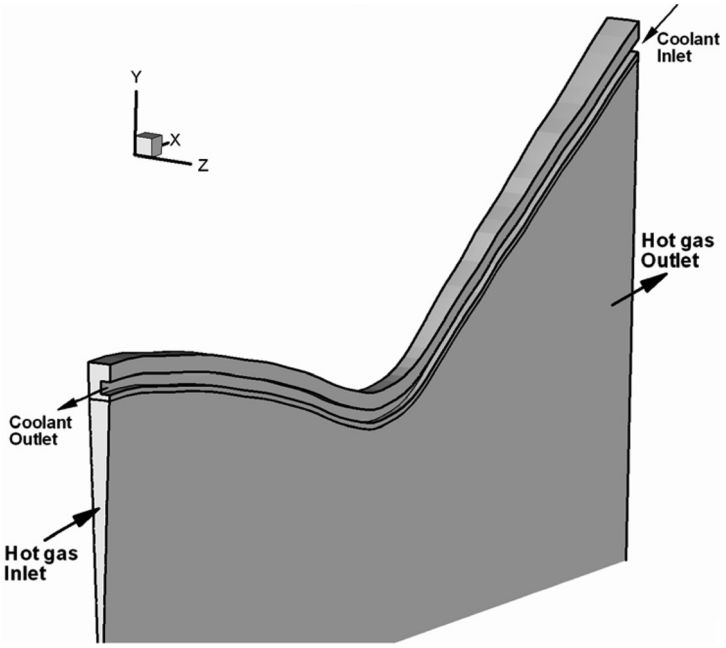

(*a*)

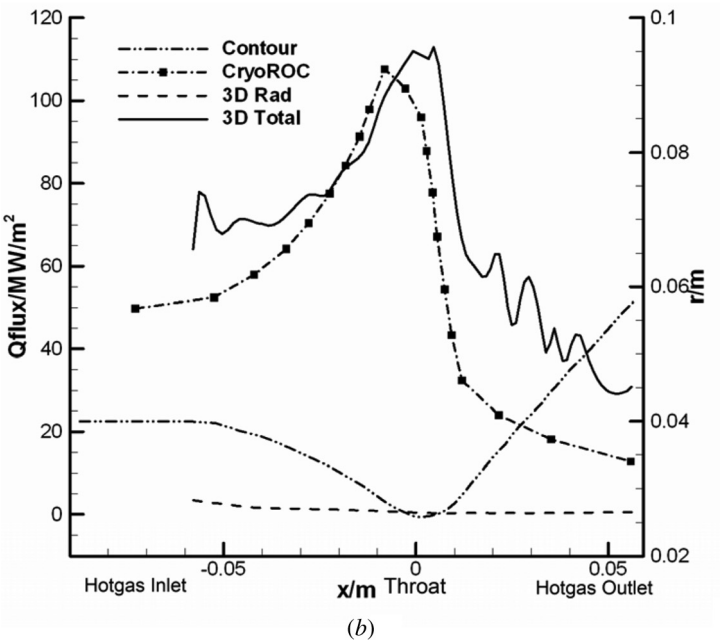

(*b*)

Figure 2. (*a*) Computational model of the test nozzle; (*b*) Comparison of experimental and computational heat flux distributions on the gas-side wall.

has the largest value at the nozzle inlet. The total heat flux at the nozzle inlet is $80\,MW/m^2$. The radiative heat flux is $4.8\,MW/m^2$, accounting for only 6% of the total heat flux. Accordingly, radiation heat transfer is neglected in the following computation.

5. RESULTS AND DISCUSSION

In this section, the baseline nozzle is analyzed numerically and the heat transfer characteristics are obtained. Three structural parameters (round-to-rectangular transforming location, height-to-width ratio of the exit plane, corner radius of the exit plane) are investigated. For each parameter, under conditions of all other geometric parameters fixed, its value is varied and three other RR nozzles are designed. Effects of this parameter on heat transfer of RR nozzles are studied and compared with the baseline.

5.1. Working Condition

For the convenience of comparison, the working conditions of all RR nozzles are the same. Chamber pressure $P_c = 3.85\,MPa$, mixture ratio $O/F = 6$. According to thermodynamic calculation, chamber temperature $T_c = 3{,}427\,K$, specific heat ratio of gas $\gamma = 1.2$, specific heat at constant pressure $C_p = 3{,}823\,J/kg\,K$, mean molecular weight is $13.15\,g/mol$. It is assumed that all hydrogen entering into the chamber is used to cool the nozzle. The flow rate of the liquid hydrogen is $0.457\,kg/s$, its temperature at the channel inlet is 30 K, and the back pressure is 4.68 MPa at the outlet.

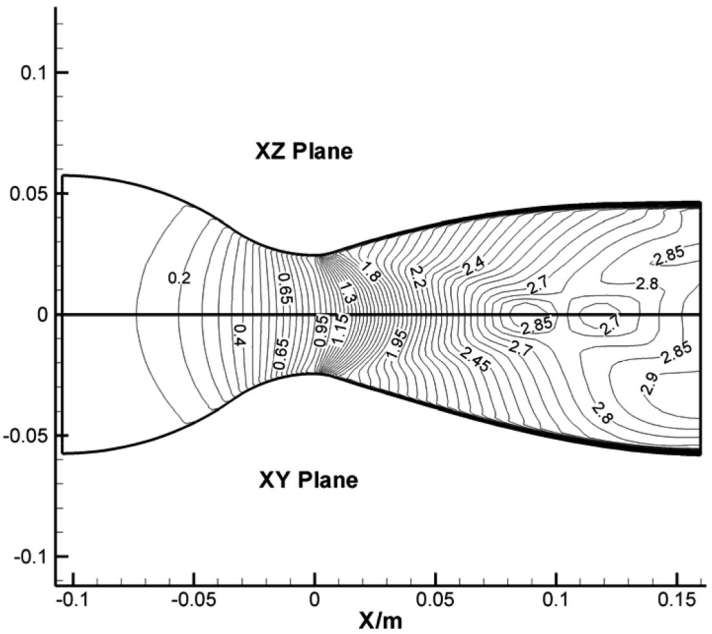

Figure 3. Mach contour in the symmetric planes of the baseline nozzle.

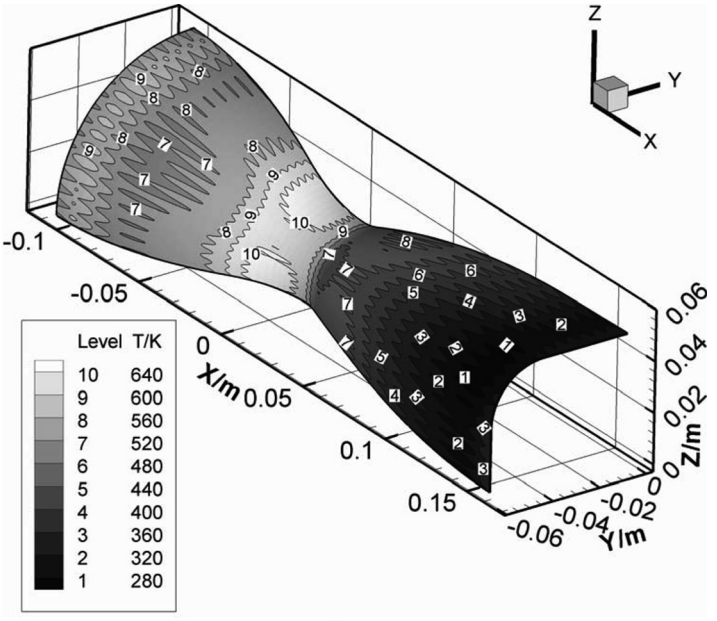

(*a*)

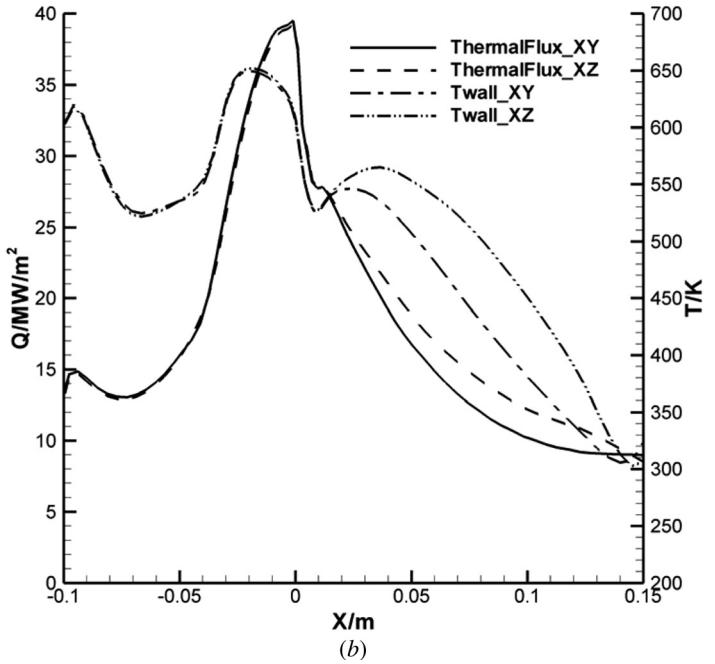

(*b*)

Figure 4. (*a*) Gas-side wall temperature field in the baseline nozzle; (*b*) Gas-side wall temperature and heat flux in the baseline nozzle.

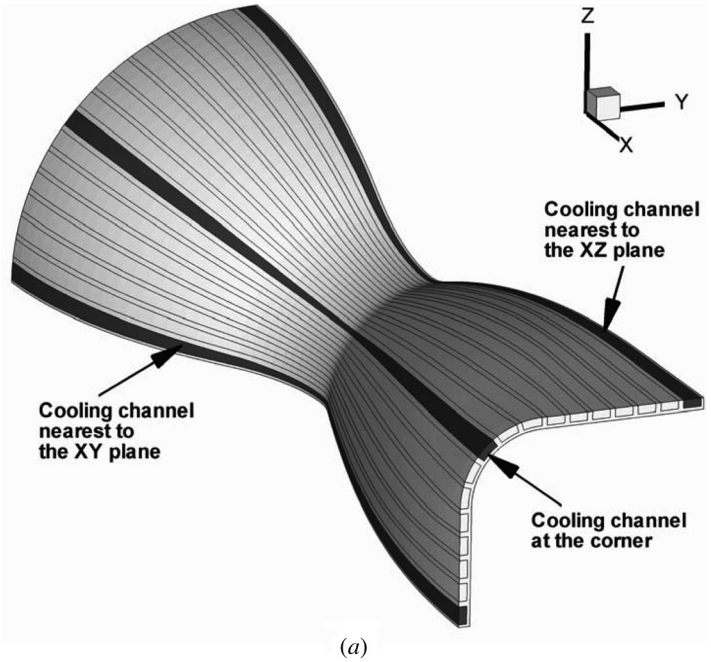

(*a*)

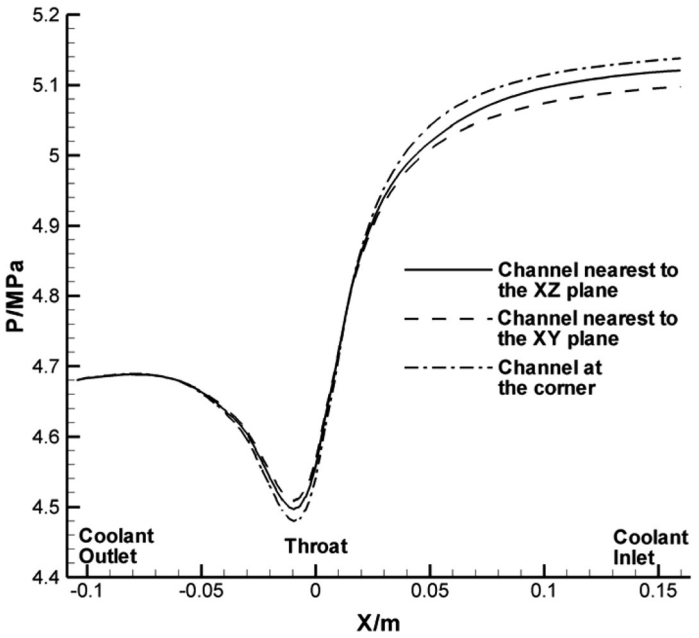

(*b*)

Figure 5. (*a*) Cooling channels used for comparison; (*b*) Pressure drop of the three channels in the baseline nozzle.

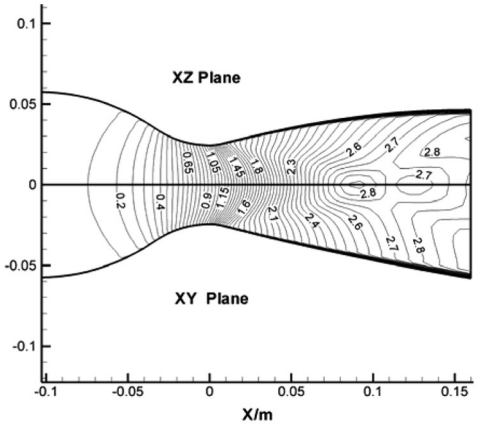

(*a*) Throat

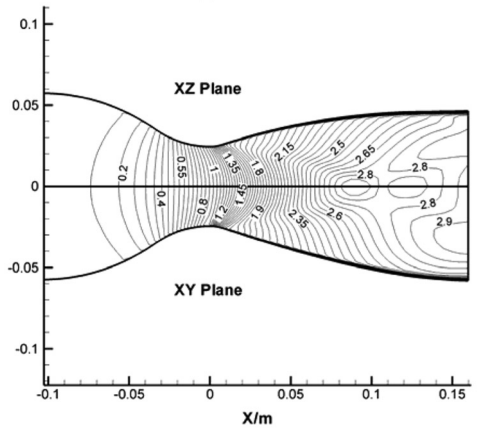

(*b*) 4.74%

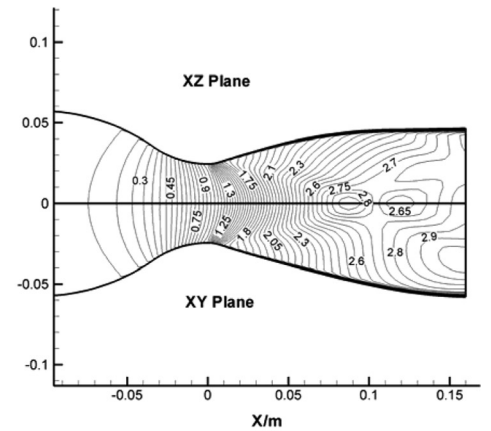

(*c*) 25%

Figure 6. Mach numbers of nozzles with different transforming positions.

Table 1. Performances of RR nozzles with different transforming positions

Transforming position	Throat	4.74%	10% (baseline)	25%
I_{sp} (m/s)	3.35417E + 03	3.35538E + 03	3.35541E + 03	3.34816E + 03
Thrust (N)	2.68679E + 03	2.68711E + 03	2.68140E + 03	2.68133E + 03
η_{Thrust}	9.76184E − 01	9.76298E − 01	9.74223E − 01	9.74200E − 01

Thermophysical properties [23] of liquid hydrogen are fitted to functions of temperature. The liner and ribs are made of ZrCu alloy, whose conductivity [24] is fitted to functions of temperature, and the outer layer of the cooling channel is electronically deposited with nickel.

5.2. Flow and Heat Transfer in the Baseline Nozzle

Mach contours in the XY and XZ planes are shown in Figure 3, which shows that flow fields in these two planes are very smooth and there is no sudden change of Mach number. Figure 4*a* is the temperature field on the gas-side wall. It shows that temperature at the nozzle inlet and throat is higher than that at other locations. At any section, temperature along the gas-wall circumference is also different and has features of three-dimensional distribution. In addition, the temperature distribution on the gas-side wall is like waves because the ribs between channels enhances heat transfer of coolant and, at the same section, temperature on the gas-side wall near the rib is lower than that on the gas-side wall beneath the cooling channel.

The temperature and heat flux at the intersections of the gas-side wall and the XY and XZ planes are plotted in Figure 4*b*. In this figure, ThermalFlux_XY and ThermalFlux_XZ stand for the wall heat flux on the XY and XZ planes, respectively. Similarly, Twall_XY and Twall_XZ represent the wall temperature on the XY and XZ planes, respectively. The figure shows that heat flux reaches its highest at the throat and declines toward upstream and downstream directions. Because the gas-side wall in the XZ plane is narrower than that in the XY plane at the divergent segment, the wall heat flux in the XZ plane is higher than that in the XY plane. From the comparison of temperature, it can be seen that there are two temperature peaks near the throat, and the wall temperature in the XZ plane is higher. The reason is that the outlines of the gas-side wall in the XY and XZ planes are S-shaped, and their curvatures change abruptly at the throat, which alters coolant flow direction and affects heat transfer.

Because the RR nozzle has a three-dimensional structure, flow conditions in cooling channels at different locations are not same. Consequently, three cooling channels are extracted. They are the cooling channels nearest to the XY plane, nearest to the XZ plane, and above the corner of the rectangular section, as shown in Figure 5*a*. Figure 5*b* illustrates the pressure distributions in these cooling channels. The horizontal coordinate represents the location along the centerline of the RR nozzle, and the vertical axis is the mean pressure in the cooling channels. Pressure distributions in the three channels share the same feature that the highest pressure occurs at the coolant inlet, the lowest at the throat, and pressure rises to the same level at the coolant outlet. The pressure difference occurs at the inlet section, the

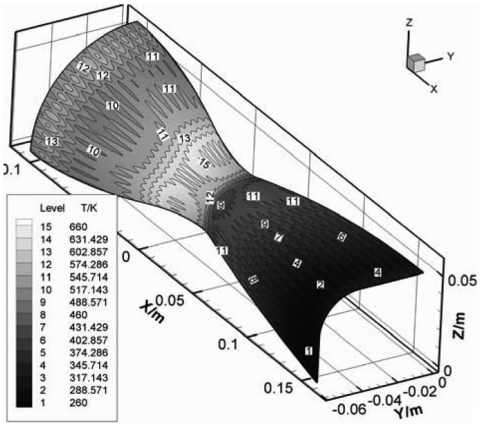

(*a*) Throat

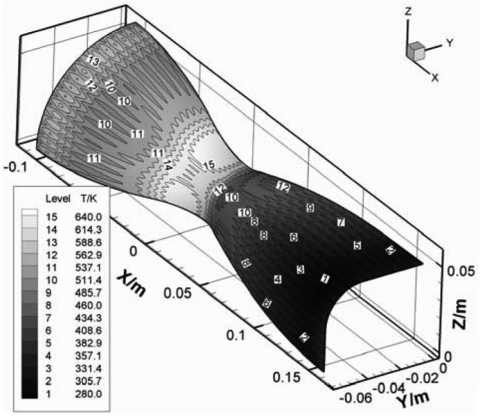

(*b*) 4.74%

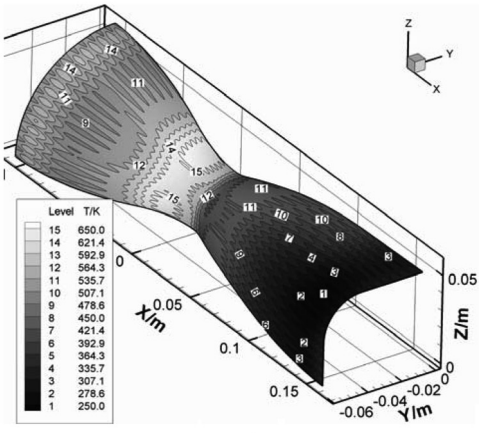

(*c*) 25%

Figure 7. Gas-side wall temperature in nozzles with different transforming positions.

channel above the corner has the highest pressure, and the channel nearest the XY plane has the lowest. The maximum difference of pressure is 0.04 MPa. However, at the throat section, pressure distribution along the circumference is reversed and the maximum pressure difference is 0.03 MPa. It can also be seen in Figure 5*b* that the lowest pressure in cooling channels occurs not at the throat, but someplace upstream of the throat. This is because the direction of the cooling channels is altered, which leads to coolant accelerating at the throat and reaching the highest velocity at some position upstream of the throat.

5.3. Effect of Round-to-Rectangular Location

In addition to the baseline transforming at 10% divergent length downstream of the throat, three other locations are chosen. They are at the throat, and 4.74% and 25% divergent length downstream of the throat.

Figure 6 shows Mach number in the symmetric planes of these nozzles. On the upper part is the Mach contour in the XZ plane; on the lower part is the Mach contour in the XY plane. The horizontal coordinates are the location along the centerline of the RR nozzle, and the origin is located at the nozzle throat. Comparing Figure 3 with Figure 6, there are smooth flow field in all four RR nozzles and no violent variation of Mach in the flow fields. This is beneficial for heat transfer.

Table 1 compares the performances of the four nozzles. Except for the nozzle that transforms at the throat, when the transforming location moves downstream, the performance of the nozzle decreases slightly. The temperature fields on the gas-side wall of the other three nozzles are similar to that of the baseline nozzle in Figure 7. The highest temperature in the four nozzles is at the level of approximately 650 K, and occurs at almost the same place. Consequently, it is concluded that the

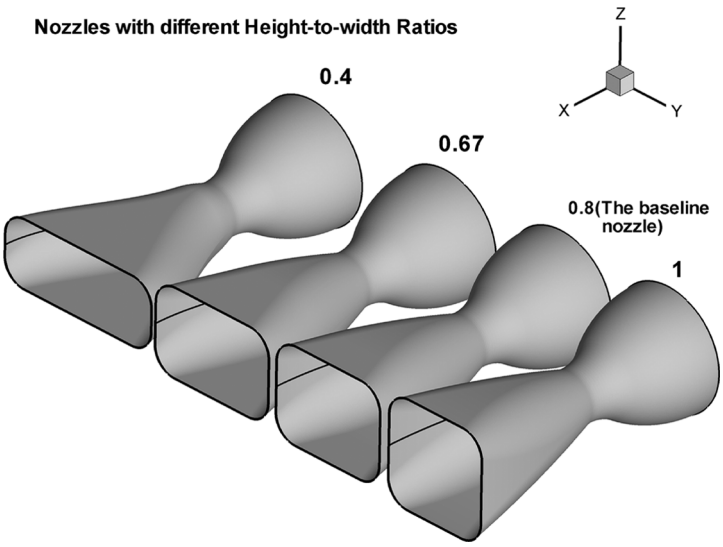

Figure 8. Contours of RR nozzles with different height-to-width ratios.

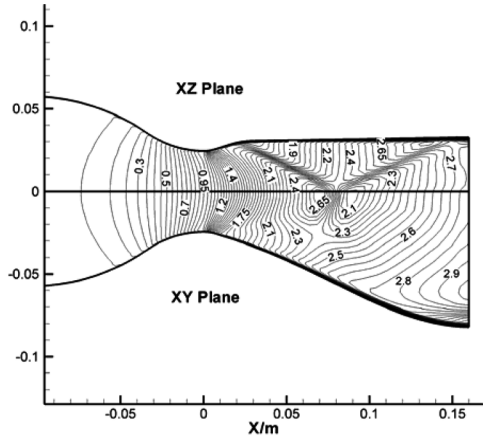

(*a*) 0.4

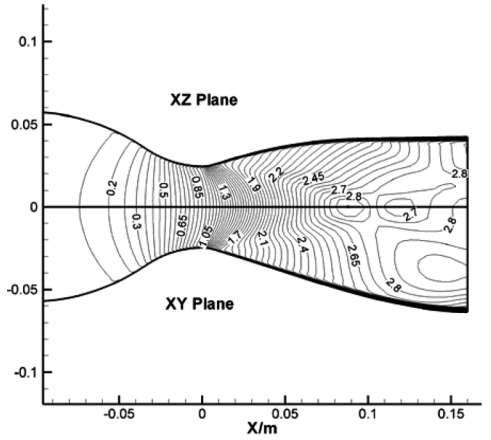

(*b*) 0.67

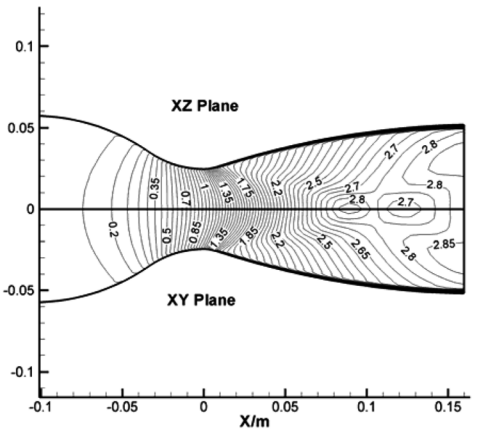

(*c*) 1

Figure 9. Mach numbers of nozzles with different height-to-width ratios.

Table 2. Performance of RR nozzles with different height-to-width ratios

Height-to-width ratio	0.4	0.67	0.8 (baseline)	1
I_{sp} (m/s)	3.25098E + 03	3.34064E + 03	3.35541E + 03	3.36093E + 03
Thrust (N)	2.60393E + 03	2.66942E + 03	2.68140E + 03	2.68490E + 03
η_{Thrust}	9.46078E − 01	9.69873E − 01	9.74223E − 01	9.75497E − 01

different locations of the round-to-rectangular tranformation do not significantly change heat transfer in the RR nozzle.

5.4. Effect of Height-to-Width Ratio at Exit

In addition to the baseline with height-to-width ratio 0.8, three nozzles with ratios of 0.4, 0.67, and 1 are chosen and studied. These four nozzles are shown in Figure 8.

Figure 9 displays Mach contours in symmetric planes for these three RR nozzles. Figure 3 and Figure 9 indicate that with increase of height-to-width ratio, the Mach contour in the XZ plane gradually becomes similar to that in the XY plane. Because the gas-side wall in the 0.4 RR nozzle in the Z direction is the flattest and transforms abruptly, this significantly affects the flow field in this nozzle. In Figure 9*a*, there is a clear compression wave. For other three nozzles, because of smooth conversion of the gas-side wall in the Z direction, no compression wave is found.

Table 2 compares the performance of the four nozzles and indicates that an increase of height-to-width ratio leads to an increase of thrust. It shows that variation of the height-to-width ratio alters the flow structure in nozzles, hence affects the nozzle performance.

Figure 10 shows the temperature fields on the gas-side wall in the three RR nozzles other than the baseline nozzle. The temperature fields are different from each other. For the nozzle with ratio equal to 0.4, deflection of the gas-side wall in the Z direction leads to a strong compression wave in the flow field and raises pressure and temperature after the wave. Consequently, a high-temperature point occurs on the gas-side wall and is almost 500 K, but is still lower than that of safe working condition. Just downstream of this point, the upper compression wave and the lower one impinge on each other, and then are reflected to form two shock waves toward the gas-side wall. Pressure and temperature behind the shock wave increase sharply and induce a second high-temperature point on the gas-side wall. The highest temperature is 1,300 K and greatly exceeds the limit that ZrCu alloy can endure.

For the other three RR nozzles, with increase of the ratio, the gas-side wall in the Z direction expands outward, which reduces the temperature on the gas-side wall just behind the transforming position. For the nozzle with a ratio of 0.67, the wall temperature in the XZ plane is higher than that of the nozzles with ratios of 0.8 and 1. In addition, with increase of the ratio, temperature distribution along the perimeter on the gas-side wall becomes more uniform.

Figure 11 shows pressure drop in the cooling channels, which indicates that the ratio of height to width has a great effect on pressure drop in the cooling channels.

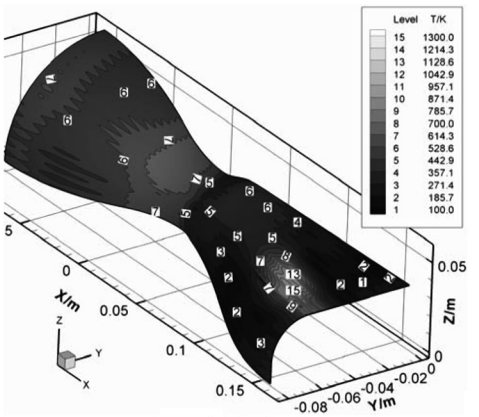

(*a*) 0.4

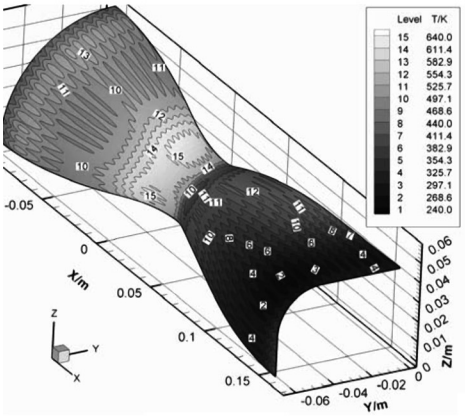

(*b*) 0.67

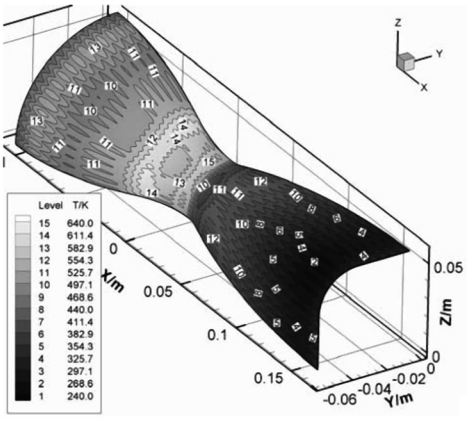

(*c*) 1

Figure 10. Gas-side wall temperature in nozzles with different height-to-width ratios.

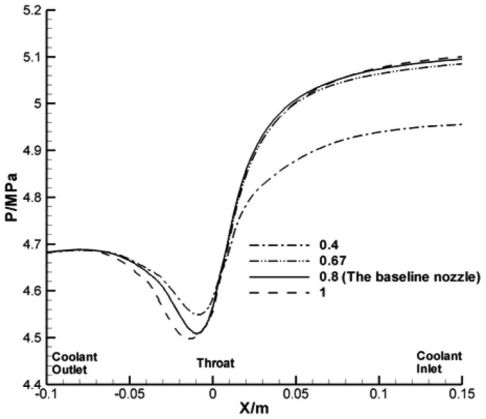

(*a*) The channel nearest to the XY plane

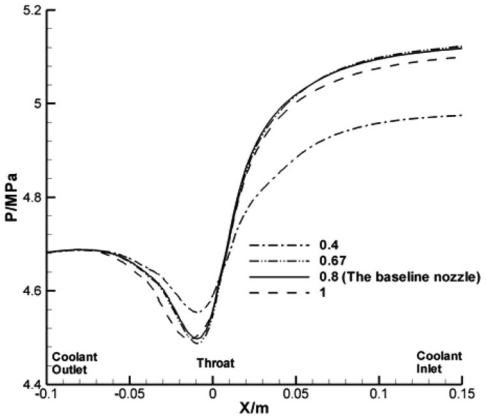

(*b*) The channel nearest to the XZ plane

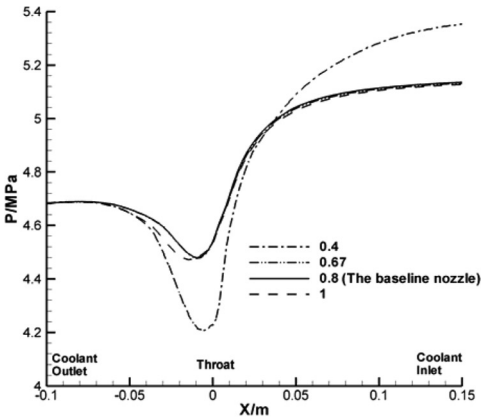

(*c*) The channel at the corner

Figure 11. Pressure drops in channels of nozzles with different height-to-width ratios.

Table 3. Performance of RR nozzles with different corner radii

Corner radius (mm)	12	17	22 (baseline)	27
I_{sp} (m/s)	3.35031E + 03	3.35221E + 03	3.35541E + 03	3.35548E + 03
Thrust (N)	2.68705E + 03	2.68852E + 03	2.68140E + 03	2.69122E + 03
η_{Thrust}	9.76276E − 01	9.76810E − 01	9.77741E − 01	9.77791E − 01

For the RR nozzle with a ratio of 0.4, inconsistency in the derivative of the gas-side wall in the XZ plane affects the heat transfer near the gas-side wall, which leads to coolant temperature and pressure becoming very high at the corner. However, coolant temperature and pressure nearest the XY and XZ planes are relatively low. In the RR nozzles with ratios larger than 0.4, their flow fields are not disturbed and the pressure drops in the channels are almost the same.

The above results indicate that (1) the ratio of height to width cannot be too small, otherwise the derivative of the gas-side wall will be inconsistent and hence the flow field will be disturbed. If there is a compression wave, a high-temperature point occurs on the gas-side wall, which endangers the working nozzle. In addition, too small a ratio affects the heat transfer in the channels, and raises the pressure drop in the channels. (2) With increase of the ratio, the flow field in the RR nozzles becomes smooth, which is advantageous to heat transfer and improves the performance of the nozzle.

5.5. Effect of Corner Radius

Based on the baseline with a corner radius of 22 mm, three RR nozzles with radii of 12, 17, and 27 mm were designed and studied. Since the gas-side walls in the XY and XZ planes in the four nozzles have almost the same profile, Mach contours in the XY and XZ planes do not vary much. Therefore, the performance difference of these nozzles is caused by the variation of corner radius. Table 3 suggests that with the expansion of the corner, the flow fields in the nozzles become smoother and their performance becomes better.

Figure 12 illustrates the temperature fields on the gas-side wall in these nozzles. Because the gas velocity near the corner is lower than that near the straight wall, the boundary layer at the corner becomes thicker, and the heat transfer from hot gas to wall is weakened. Furthermore, the corner radii also affect the temperature distribution on the perimeter at the throat section. The nozzle with a corner radius of 12 mm has the most nonuniform temperature distribution on the perimeter at the throat section. In this nozzle, the temperature on the gas-side wall in the XY and XZ planes is higher than that at the corner. In contrast, in the nozzle with a corner radius of 27 mm, the temperature along the perimeter of the gas-side wall at the throat is nearly the same.

Pressure drops in cooling channels are plotted in Figure 13. Figure 13*a* and 13*b* imply that the four nozzles have very similar coolant pressure drops near the XY and XZ planes because the outline of the gas-side wall in the XY and XZ planes is the same. However, in Figure 13*c*, since the nozzle with a corner radius of 12 mm has the smallest corner, the length of the generatrix at the corner is the largest, and

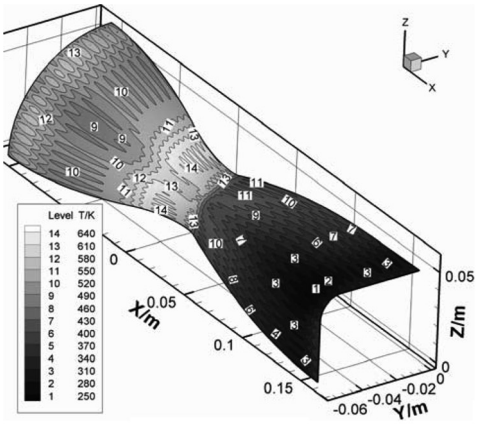

(*a*) R12

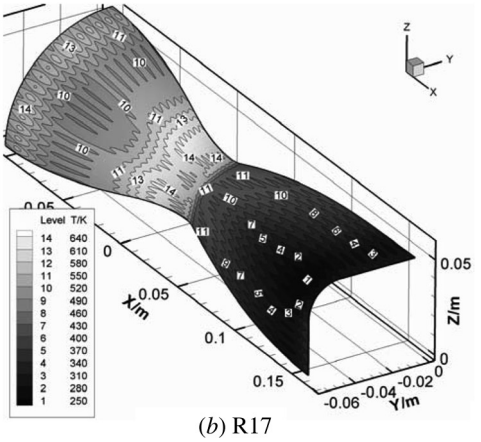

(*b*) R17

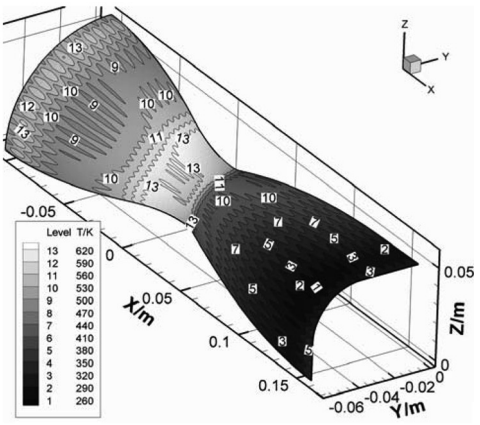

(*c*) R27

Figure 12. Gas-side wall temperature in nozzles with different corner radii.

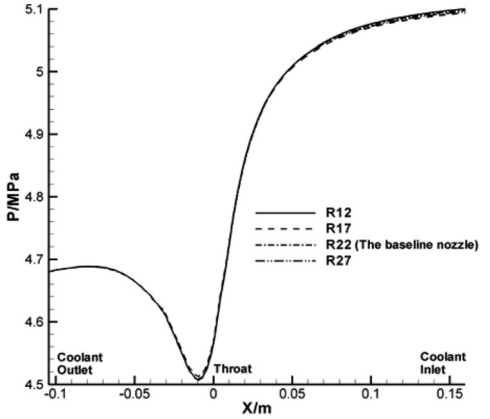

(*a*) The channel nearest to the XY plane

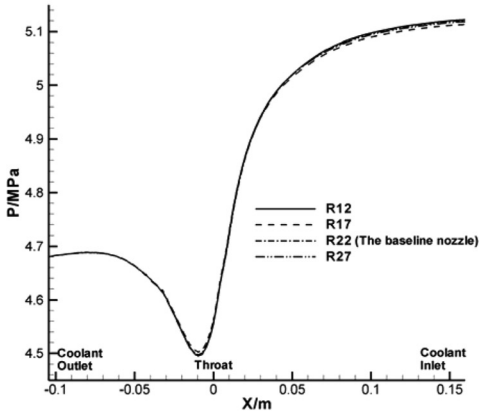

(*b*) The channel nearest to the XZ plane

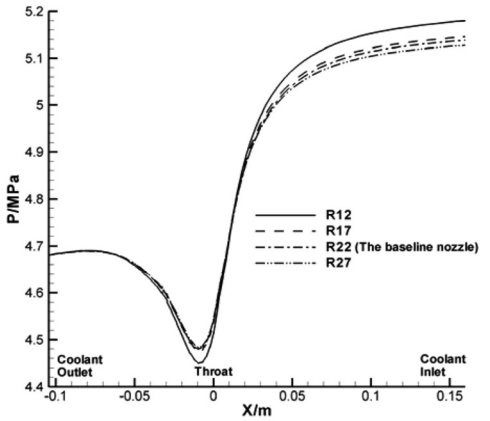

(*c*) The channel at the corner

Figure 13. Pressure drops in channels of nozzles with different corner radii.

the pressure drop in channels at the corner is also the largest. With increase of the corner radius, the pressure drop in the channels at the corner decreases.

The above results show that (1) the corner radius has an influence on the heat transfer in the RR nozzle. Large radius makes temperature on the perimeter at the divergent segment uniform, and weakens the three-dimensional feature of the temperature distribution on the gas-side wall. (2) The corner radius affects the smoothness of the flow field. Small radius could increase nonaxisymmetric loss, and therefore lower the thrust of RR nozzles.

6. CONCLUSION

A three-dimensional numerical procedure has been carried out to examine the flow and heat transfer in RR nozzles. The results are summarized as follows.

1. The RR nozzle has three-dimensional structure and also has a three-dimensional thermal field. At any section normal to the centerline, temperatures on the perimeter of gas-side wall are different. Ribs between cooling channels enhance heat transfer between the solid wall and coolant and make temperature fluctuate on the gas-side wall. Wall temperature near ribs is lower than that under the bottom of the cooling channel.
2. Under the condition that the derivative of the surface contour is consistent, the transforming position has little influence on flow and heat transfer and the four RR nozzles have similar performance.
3. The ratio of height to width at the outlet greatly affects flow and heat transfer in RR nozzles. Too small a ratio disturbs the flow field in RR nozzles and leads to a high temperature point, even burning out nozzles. The choice of height-to-width ratio should ensure smoothness and no sharp discontinuity in the flow field.
4. The corner radius influences the temperature field on the gas-side wall. The smaller the corner radius, the larger the pressure loss in cooling channels.

REFERENCES

1. J. M. Kazaroff and A. J. Pavli, Advanced Tube-Bundle Rocket Thrust Chamber, AIAA 90–2726, 1990.
2. A. Fröhlich, M. Popp, G. Schmidt, and D. Thelemann, Heat Transfer Characteristics of H_2/O_2-Combustion Chambers, AIAA 93–1826, 1993.
3. D. K. Huzel and D. H. Huang, *Modern Engineering for Design of Liquid-Propellant Rocket Engines*, AIAA Progress in Astronautics and Aeronautics, vol. 147, 1992.
4. C. H. Marchi, F. Laroca, A. F. C. Silva, and J. N. Hinckel, Numerical Solutions of Flows in Rocket Engines with Regenerative Cooling, *Numer. Heat Transfer A*, vol. 45, pp. 699–717, 2004.
5. M. Popp and G. Schmidt, Heat Transfer Investigations for High Pressure Rocket Combustion Chambers, AIAA 94–3102, 1994.
6. T. S. Wang and V. Luong, Hot-Gas-Side and Coolant-Side Heat Transfer in Liquid Rocket Engine Combustors, *J. Thermophys. Heat Transfer*, vol. 8, pp. 524–530, 1994.
7. T. S. Wang, A. Droege, M. D. Agostino, Y. C. Lee, and R. Williams, Asymmetric Base-Bleed Effect on Aerospike Plume-Induced Base-Heating Environment, *J. Propulsion Power*, vol. 20, pp. 385–393, 2004.

8. A. Fröhich, H. Immich, F. LeBail, and M. Popp, Three-Dimensional Flow Analysis in a Rocket Engine Coolant Channel of High Depth/Width Ratio, AIAA 91–2183, 1991.
9. F. Le Bail and M. Popp, Numerical Analysis of High Aspect Ratio Cooling Passage Flow and Heat Transfer, AIAA 93–1829, 1993.
10. O. Knab, A. Fröhlich, D. Wennerberg, and W. Haslinger, Advanced Cooling Circuit Layout for the VINCI Expander Cycle Thrust Chamber, AIAA 2002–4005, 2002.
11. T. S. Park, Numerical Study of Turbulent Flow and Heat Transfer in a Convex Channel of a Calorimetric Rocket Chamber, *Numer. Heat Transfer A*, vol. 45, pp. 1029–1047, 2004.
12. T. E. Booth, J. O. Vilja, D. P. Cap, and R. J. McGill, The Design of Linear Aerospike Thrust Cells, AIAA 93–2562, 1993.
13. G. Hagemann, H. Immich, and G. Dumnov, A Critical Assessment of the Linear Plug Nozzle Concept, AIAA 2001–3683, 2001.
14. J. Liu, H. M. Shang, Y. S. Chen, and T. S. Wang, Prediction of Radiative Transfer in General Body-Fitted Coordinates, AIAA 97–0811, 1997.
15. B. Leckner, Spectral and Total Emissivity of Water Vapor and Carbon Dioxide, *Combustion and Flame*, vol. 19, pp. 33–48, 1972.
16. D. R. Ballal, Estimation and Optimization of the Film Cooling Requirements in a Gas Turbine Combustion Chamber, *CRANFIELD-SME-5*, 1973.
17. *Fluent User's Manual*, Version 6.0, November 2001.
18. D. Preclik, D. Wiedmann, W. Oechslein, and J. Kretschmer, Cryogenic Rocket Calorimeter Chamber Experiments and Heat Transfer Simulations, AIAA 98–3440, 1998.
19. H. Immich, T. Frohlich, and J. Kretschmer, Technology Developments for Expander Cycle Engine Thrust Chambers, AIAA 99–2889, 1999.
20. H. Immich, J. Kretschmer, and D. Preclik, Technology Developments for Cryogenic Rocket Engines, AIAA 2000–3780, 2000.
21. H. Immich, J. Alting, J. Kretschmer, and D. Preclik, Technologies for Thrust Chambers of Future Launch Vehicle Liquid Rocket Engines, AIAA 2002–4143, 2002.
22. M. Popp and G. Schmidt, Rocket Engine Combustion Chamber Design Concepts for Enhanced Life, AIAA 96–3303, 1996.
23. Feng Wang, *Thermal Properties of Liquid and Gas*, pp. 246–273, National Defense Industry Press, Beijing, 1980 (in Chinese).
24. Guoqiu Liu, *Fundamental of Liquid Rocket Engine*, pp. 341–342, China Astronautics Publishing House, Beijing, 1993 (in Chinese).

Copyright of Numerical Heat Transfer: Part A -- Applications is the property of Taylor & Francis Ltd and its content may not be copied or emailed to multiple sites or posted to a listserv without the copyright holder's express written permission. However, users may print, download, or email articles for individual use.

Copyright of Numerical Heat Transfer: Part A -- Applications is the property of Taylor & Francis Ltd and its content may not be copied or emailed to multiple sites or posted to a listserv without the copyright holder's express written permission. However, users may print, download, or email articles for individual use.